Fluid Phase Equilibria 362 (2014) 335–341

Contents lists available at ScienceDirect

Fluid Phase Equilibria

journal homepage: www.elsevier.com/locate/fluid

Phase equilibrium of fluids confined in porous media from an extended Peng–Robinson equation of state

Leonardo Travalloni[a], Marcelo Castier[b,*], Frederico W. Tavares[a,c]

[a] Escola de Química, Universidade Federal do Rio de Janeiro, Rio de Janeiro C.P. 68542, Brazil
[b] Chemical Engineering Program, Texas A&M University at Qatar, P.O. Box 23874 Doha, Qatar
[c] Programa de Engenharia Química – COPPE, Universidade Federal do Rio de Janeiro, Rio de Janeiro, C.P. 68542, Brazil

ARTICLE INFO

Article history:
Received 30 June 2013
Received in revised form
26 September 2013
Accepted 24 October 2013
Available online 1 November 2013

Keywords:
Confined fluid
Porous media
Equation of state
Multiphase equilibrium
Heterogeneity

ABSTRACT

Fluid behavior in nanometric cavities and in bulk phases may be remarkably different but there is a dearth of simple analytical models that can predict such difference with a single set of parameters. In this work, commonly used cubic equations of state are extended to the modeling of fluids confined in porous media. A model based on the Peng–Robinson equation of state is used to study the phase equilibrium of pure fluids and mixtures confined in homogeneous and heterogeneous porous media. The problem is formulated as a multiphase equilibrium calculation because each kind of pore in a heterogeneous porous media has its own confinement effect and may contain one or more phases with unique properties. The specifications are the temperature, the total amount of each fluid component, the volume available for bulk phases, and the total volume of each kind of pore, so that the equilibrium condition is the minimum Helmholtz energy. The global phase stability test is executed to assess the need for phase additions. Results illustrate the potential of the model and of the multiphase equilibrium algorithm, by predicting different phase configurations under confinement. Each kind of pore may confine phases with very similar or very different densities and compositions. Furthermore, it is shown that the methodology of this work can predict the formation of transition regions like those of oil reservoirs.

1. Introduction

Confinement in small scales changes fluid properties due to geometric constraints imposed on fluid molecules and interaction between these molecules and the pore walls (molecule–wall interaction). As an example, confinement may shift the phase transitions of a fluid, so that the confined fluid in equilibrium with a given bulk phase may be either a gas-like or a liquid-like phase, depending on the pore size and on the molecule–wall interaction energy [1,2]. In natural oil reservoirs, these effects give rise to transition regions known as GOC (gas–oil contact) and WOC (water–oil contact), where phases with different densities coexist at the same vertical level of the porous rock, due to its heterogeneity [3]. The occurrence of transition regions can be attributed to a variable capillary pressure through the reservoir because of different molecule–wall interactions in structurally or chemically distinct pores. The prediction of this phenomenon is important for oil recovery processes.

A detailed description of the local properties of confined fluids demands sophisticated approaches, such as molecular simulation techniques [4]. However, these techniques still have large computational cost, hindering their application to process simulation problems. Another approach, simplistic but with minimum computational cost, is the use of traditional adsorption isotherm models. Nevertheless, this approach combines different models for the bulk and adsorbed phases [5] and is unable to describe phase transition behavior between the confined and bulk states with a single set of parameters.

A third approach, developed more recently, is the use of an analytical equation of state that represents the main effects of confinement explicitly. This kind of model allows a continuous and self-consistent description of the fluid global properties as a function of the system dimensions. Besides, if the same equation of state is valid for bulk and confined fluids, existing algorithms for phase equilibrium calculations can be readily adapted to solve general adsorption equilibrium problems. Few models of this kind were proposed in the literature [6–8] and none of them is sufficiently accurate, in a large range of conditions, for application in engineering problems. One important application would be the prediction, with a single model, of the equilibrium distribution of oil and natural gas in the highly heterogeneous structures of shale reservoirs,

* Corresponding author. Tel.: +974 4423 0534.
E-mail addresses: marcelo.castier@qatar.tamu.edu, mcastier@gmail.com (M. Castier).

0378-3812/$ – see front matter © 2013 Elsevier B.V. All rights reserved.
http://dx.doi.org/10.1016/j.fluid.2013.10.049

in order to promote their recovery from these potential energy supplies [9].

In our previous work [10], an extension of the van der Waals equation of state was developed for modeling the behavior of confined fluids as an explicit function of pore size and of the molecule–wall interaction. Therefore, the same model could be used for both adsorbed and bulk phases, providing a consistent description of adsorption systems. This model describes different types of adsorption isotherms and several features of the confined fluid critical behavior [11] as predicted by theoretical work in the literature, like the emergence of a second critical point [12].

In this work, the same methodology used to extend the van der Waals model to confined fluids was applied to other cubic equations of state. The model obtained from the Peng–Robinson equation of state was used in a multiphase equilibrium calculation algorithm in order to investigate the phase configurations of pure fluids and mixtures confined in homogeneous and heterogeneous porous media.

2. Equations of state for confined fluids

The formulation of the model based on the van der Waals equation of state is discussed in detail elsewhere [10]. Here, we follow a similar modeling approach, which we summarize, focusing on the differences among the confined fluid models obtained from other equations of state.

Model development was guided by the generalized van der Waals theory [13,14]. The starting point is the canonical partition function (Q), from which all thermodynamic properties of a closed system can be obtained:

$$Q(T, V, N_1, N_2, \ldots N_{NC}) = \prod_{i=1}^{NC} \left(\frac{q_i^{N_i}}{\lambda_i^{3N_i} N_i!} \right) V_f^N \exp\left(\int_{\infty}^{T} \frac{E_{conf}}{kT^2} dT \right)$$

where T is the temperature, V is the total volume, N is the total number of molecules in the fluid mixture, NC is the number of fluid components, index i denotes a component, q and λ are intramolecular and translational contributions, respectively, k is the Boltzmann constant, V_f is the free volume, and E_{conf} is the configurational energy. The system description is completed by assuming models for V_f and E_{conf}, which determine the repulsive and the attractive parts of the equation of state, respectively.

Assuming the classic mixing rule for the volume parameter of the equation of state, V_f is modeled by:

$$V_f = V - \sum_{i=1}^{NC} \left(\frac{N_i}{\rho_{\max,i}} \right)$$

where $\rho_{max,i}$ is the packing density of pure component i, whose dependence on pore size was obtained by fitting literature data [15] of hard spheres packed in cylinders:

$$\rho_{\max,i}\sigma_i^3 = c_1 - c_2 \exp\left(c_3 \left(0.5 - \frac{r_p}{\sigma_i} \right) \right) + c_4 \exp\left(c_5 \left(0.5 - \frac{r_p}{\sigma_i} \right) \right)$$

where σ_i is the molecular diameter of component i, r_p is the pore radius, and the fitting constants are $c_1 = 1.158$, $c_2 = 0.479$, $c_3 = 0.621$, $c_4 = 0.595$, and $c_5 = 4.014$. For consistency with the packing density predicted by the equation of state which is being extended to confined fluids, σ_i must be calculated from the bulk volume parameter (b_i) by [10]:

$$\sigma_i = \sqrt[3]{\frac{c_1}{N_{av}} b_i}$$

where N_{av} is the Avogadro number.

Table 1
Coordination number model for different bulk equations of state.

Equation of state	$N^b_{c,ij}$ Model
van der Waals	$cx_i\rho$
Redlich–Kwong	$\frac{d}{\sqrt{T}} \frac{x_i\rho_{\max}}{\sqrt{\rho_{\max,i}\rho_{\max,j}}} \ln\left(1 + \frac{\rho}{\rho_{\max}}\right)$
Soave	$f_{S,ij}(T) \frac{x_i\rho_{\max}}{\sqrt{\rho_{\max,i}\rho_{\max,j}}} \ln\left(1 + \frac{\rho}{\rho_{\max}}\right)$
Peng–Robinson	$f_{PR,ij}(T) \frac{x_i\rho_{\max}}{\sqrt{\rho_{\max,i}\rho_{\max,j}}} \ln\left(\frac{1+(1+\sqrt{2})\rho/\rho_{\max}}{1+(1-\sqrt{2})\rho/\rho_{\max}}\right)$

Most of the cubic equations of state in common use differ only in the attractive part, which depends on the E_{conf} model. Considering that the pairwise interaction of fluid molecules (molecule–molecule interaction) occurs through a square well potential, the molecule–wall interaction occurs through another square well potential, and the interaction potentials of all fluid components are pairwise additive, E_{conf} was modeled by [10]:

$$E_{conf} = -\sum_{i=1}^{NC}\sum_{j=1}^{NC} \left(\frac{N_j}{2} N_{c,ij} \varepsilon_{ij} \right) - \sum_{i=1}^{NC} \left(N_i F_{p,i} \varepsilon_{p,i} \right)$$

where ε_{ij} is the intermolecular interaction energy between components i and j, $\varepsilon_{p,i}$ is the interaction energy between one molecule of component i and the entire pore wall, $N_{c,ij}$ is the coordination number (i.e., the number of molecules of component i that coordinate with a central molecule of component j), and $F_{p,i}$ is the fraction of the confined molecules in the range of the pore wall attractive field. In the previous equation, the first term on the right hand side accounts for molecule–molecule interactions and the second one accounts for molecule–wall interactions. The term $F_{p,i}$ is intended to represent the distribution of fluid molecules inside the pore, which depends on temperature, fluid density, and geometric features of the system. This term was modeled by an empirical expression that satisfies some physical limits expected for the system [10]:

$$F_{p,i} = F_{pa,i} + \left(1 - F_{pa,i}\right) \left(1 - \exp\left(-\frac{\varepsilon_{p,i}}{kT}\right)\right) \left(1 - \frac{x_i\rho}{\rho_{\max,i}}\right)^{\theta_i}$$

where ρ is the fluid density, x_i is the mole fraction of component i, $F_{pa,i}$ is the value of $F_{p,i}$ for random distribution of the fluid molecules inside the pore:

$$F_{pa,i} = \frac{\left(r_p - \sigma_i/2\right)^2 - \left(r_p - \sigma_i/2 - \delta_{p,i}\right)^2}{\left(r_p - \sigma_i/2\right)^2}$$

θ_i is a geometric term:

$$\theta_i = \frac{r_p}{\delta_{p,i} + \sigma_i/2}$$

and $\delta_{p,i}$ is the square well width of the molecule–wall interaction potential of component i. The coordination number was also modeled by an empirical expression:

$$N_{c,ij} = N^b_{c,ij} \left(1 - \frac{2}{5}\frac{\sigma_{ij}}{r_p}\right)$$

where $N^b_{c,ij}$ is the bulk coordination number, σ_{ij} is the mean molecular diameter for components i and j, and the term in parenthesis accounts for the coordination number decrease with pore size reduction. The $N^b_{c,ij}$ expression is specific for each bulk fluid equation of state and depends on the mixing rules adopted. Table 1 shows the underlying $N^b_{c,ij}$ expressions for different bulk models, assuming classic mixing rules. In these expressions, c and d are constants, $f_{S,ij}$ and $f_{PR,ij}$ are functions of temperature, and ρ_{max} is

Table 2
Confinement-modified attractive part of different equations of state for confined fluids.

Original equation of state	Extended equation of state	ψ Term
van der Waals	vdW-C	$\frac{a_p}{v^2}$
Redlich–Kwong	RK-C	$\frac{a_p}{\sqrt{T}v(v+b_p)}$
Soave	S-C	$\frac{a_p(T)}{v(v+b_p)}$
Peng–Robinson	PR-C	$\frac{a_p(T)}{v(v+b_p)+b_p(v-b_p)}$

Table 3
Definition of the pure component energy parameter for different equations of state.

Equation of state	a_i
vdW-C	$\frac{N_{av}^2 c\varepsilon_{ii}}{2}$
RK-C	$\frac{N_{av}^2 d\varepsilon_{ii}}{3\rho_{\max,i}}$
S-C	$\frac{N_{av}^2 \varepsilon_{ii}}{2\rho_{\max,i}}\alpha_{S,i}(T)$
PR-C	$\frac{\sqrt{2}N_{av}^2 \varepsilon_{ii}}{\rho_{\max,i}}\alpha_{PR,i}(T)$

the packing density of the mixture, given by the classic mixing rule:

$$\rho_{\max} = \frac{1}{\sum_{i=1}^{NC} x_i/\rho_{\max,i}}$$

Once the partition function is completely determined, the equation of state for pressure (P) is obtained from the thermodynamic relation:

$$P = kT\left(\frac{\partial \ln Q}{\partial V}\right)_{T,N_1,N_2\ldots N_{NC}}$$

For the bulk equations of state mentioned in Table 1, the extended models have the general form:

$$P = \frac{RT}{v-b_p} - \Psi - \sum_{i=1}^{NC}\left(x_i\theta_i\frac{x_i b_{p,i}}{v^2}\left(1-\frac{x_i b_{p,i}}{v}\right)^{\theta_i-1}\left(1-F_{pa,i}\right)\right.$$
$$\left.\times\left(RT\left(1-\exp\left(-\frac{N_{av}\varepsilon_{p,i}}{RT}\right)\right)-N_{av}\varepsilon_{p,i}\right)\right) \quad (1)$$

where R is the universal gas constant, v is the molar volume of the fluid mixture, $b_{p,i}$ is the confinement-modified volume parameter of pure component i:

$$b_{p,i} = \frac{N_{av}}{\rho_{\max,i}}$$

b_p is the confinement-modified volume parameter of the fluid mixture:

$$b_p = \sum_{i=1}^{NC} x_i b_{p,i}$$

and ψ is the confinement-modified attractive part of the model, which depends on the bulk equation of state adopted as the basis for model development. Table 2 shows the nomenclature of the extended models and the corresponding ψ terms. In these expressions, a_p is the confinement-modified energy parameter of the fluid mixture:

$$a_p = \sum_{i=1}^{NC}\sum_{j=1}^{NC}(x_i x_j a_{p,ij})$$

where $a_{p,ij}$ is given by the combination rule:

$$a_{p,ij} = \sqrt{a_i a_j}\left(1-\frac{2}{5}\frac{\sigma_{ij}}{r_p}\right)$$

and a_i is the energy parameter of pure component i. Parameter a_i is defined according to Table 3, where $\alpha_{S,i}$ and $\alpha_{PR,i}$ are the conventional functions of temperature and acentric factor for the equations of state of Soave and Peng–Robinson, respectively.

From Eq. (1) and Table 2, it can be seen that each extended model has two terms similar to those present in the original equations of state, and a new, larger term. Also, there is a pair of parameters that characterize the molecule–wall interaction intensity ($\varepsilon_{p,i}$ and $\delta_{p,i}$). All the extended models reduce to the respective bulk equations of state in the limit of infinitely large pore size; therefore, they are valid for both confined and bulk fluids.

3. Multiphase equilibrium calculations

Porous solids are, in general, structurally and chemically heterogeneous, characterized by distributions of pore sizes and adsorption energies. A heterogeneous porous medium provides different regions for fluid confinement, each of them with a specific set of pore size and adsorption energy, thus influencing fluid properties in a unique way. In each of these confining regions, fluid may occur as one or more phases, depending on system conditions. Therefore, a multiphase equilibrium calculation is indicated for predicting fluid confinement in most porous solids.

In this work, a multiphase equilibrium calculation algorithm [16] was adapted for use with the PR-C equation of state, Eq. (1). The specifications were the system temperature, the total amount of each fluid component, the total volume of the bulk region and of each confining region, and the pore size and adsorption energy distributions (i.e., the pore radius and the pair of molecule–wall interaction parameters assigned to each confining region). With these specifications, the thermodynamic equilibrium condition is the minimum Helmholtz energy of the system (F):

$$F = \sum_{g=1}^{NR}\sum_{h=1}^{NF_g} F_{gh}$$

where NR is the total number of regions available to the fluid (including the bulk region), NF_g is the number of fluid phases in region g, and F_{gh} is the Helmholtz energy of phase h in region g. The contribution of each phase (bulk or confined) to F was obtained from the PR-C model by:

$$F_{gh} = -P_{gh}V_{gh} + \sum_{i=1}^{NC} n_{gh,i}\mu_{gh,i}$$

where P_{gh} and V_{gh} are the pressure and the volume of phase h in region g, respectively, and $n_{gh,i}$ and $\mu_{gh,i}$ are the mole number and the chemical potential of component i in the same phase, respectively. Minimization of F was carried out using a Newton method based algorithm [17], with variables related to the volume of each phase and to the amount of each component in each phase [18]. These variables are the volumetric fraction of each phase in its region (φ_{gh}):

$$\varphi_{gh} = \frac{V_{gh}}{V_g}$$

where V_g is the total volume of region g, and the distribution factor of each component in each phase ($\eta_{gh,i}$):

$$\eta_{gh,i} = \frac{n_{gh,i}}{n_i}$$

where n_i is the total mole number of component i. As the total volume of each region and the total mole number of each component are specifications, the following constraints can be written:

$$\sum_{h=1}^{NF_g} \varphi_{gh} = 1$$
$$\sum_{g=1}^{NR} \sum_{h=1}^{NF_g} \eta_{gh,i} = 1$$

Therefore, one volumetric fraction for each region and one distribution factor for each component can be taken as dependent variables. In the minimization algorithm, the objective function was $F/(RT)$, the elements of the gradient vector were:

$$\frac{\partial(F/(RT))}{\partial \varphi_{gh}} = \frac{V_g}{RT}\left(-P_{gh} + P_{gH}\right)$$
$$\frac{\partial(F/(RT))}{\partial \eta_{gh,i}} = \frac{n_i}{RT}\left(\mu_{gh,i} - \mu_{GH,i}\right) \quad (2)$$

and the elements of the Hessian matrix were:

$$\frac{\partial^2(F/RT)}{\partial\varphi_{gh}\partial\varphi_{st}} = \Delta_{g,s}\frac{V_g^2}{RT}\left(-\frac{\Delta_{gh,st}}{\sum_{i=1}^{NC} n_{gh,i}}\frac{\partial P_{gh}}{\partial v_{gh}} - \frac{1}{\sum_{i=1}^{NC} n_{gH,i}}\frac{\partial P_{gH}}{\partial v_{gH}}\right)$$
$$\frac{\partial^2(F/RT)}{\partial\eta_{gh,i}\partial\eta_{st,j}} = \frac{n_i n_j}{RT}\left(\left(\Delta_{gh,st} - \Delta_{gh,ST}\right)\frac{\partial\mu_{gh,i}}{\partial n_{gh,j}} - \left(\Delta_{GH,st} - \Delta_{GH,ST}\right)\frac{\partial\mu_{GH,i}}{\partial n_{GH,j}}\right)$$
$$\frac{\partial^2(F/RT)}{\partial\varphi_{gh}\partial\eta_{st,j}} = \frac{V_g n_i}{RT}\left(\left(\Delta_{gh,st} - \Delta_{gh,ST}\right)\frac{\partial P_{gh}}{\partial n_{gh,j}} - \left(\Delta_{GH,st} - \Delta_{GH,ST}\right)\frac{\partial P_{GH}}{\partial n_{GH,j}}\right)$$

where Δ is the Kronecker delta function, capital indexes indicate phases which provide the dependent variables, and all derivatives were analytically obtained from Eq. (1). The multiphase equilibrium calculation starts with a local minimization of F considering the existence of a single fluid phase in each region. Then, a global stability test is executed using the tangent plane criterion [18]. If an unstable phase is detected in a given region, a phase is inserted there and a new minimization of F is performed. Premature phase insertions may occur when using this scheme. Therefore, as F is minimized, the algorithm removes phases if such removal reduces the value of F. When all phases are stable, the problem is solved, giving the number of phases in each region and the volume, amount, and composition of each phase.

At equilibrium, the gradient vector is null. From Eq. (2), it implies that:

$$P_{gh} = P_{gH} \quad \forall h \in \left\{1, 2, \ldots NF_g\right\}$$
$$\mu_{gh,i} = \mu_{GH,i} \quad \forall g \in \{1, 2, \ldots NR\} \quad \text{and} \quad \forall h \in \left\{1, 2, \ldots NF_g\right\} \quad (3)$$

Therefore, the chemical potential of each component is the same in all phases in equilibrium, but the pressure is equal only in phases located in the same region (i.e., phases subject to the same type of confinement). Making NF the total number of fluid phases in the system, Eq. (3) gives $(NC\,(NF-1) + NF - NR)$ independent equations relating intensive variables. These variables are the temperature, the pressure in each phase, and the chemical potential of each component in each phase, totaling $(NC\,NF + 1)$ independent variables. Therefore, the number of degrees of freedom (NL) is:

$$NL = 1 + NR + NC - NF \quad (4)$$

Eq. (4) is the Gibbs phase rule extended to fluid adsorption in heterogeneous porous media, in which one degree of freedom is added for each confining region.

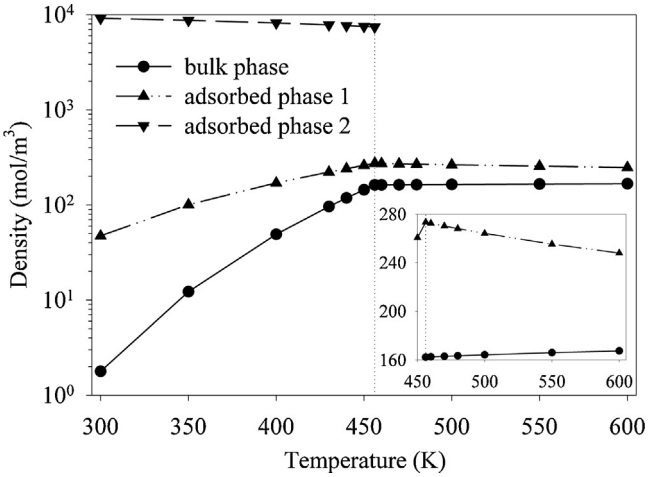

Fig. 1. Density of the fluid phases in system I as a function of temperature ($r_p/\sigma = 26.48$, $\varepsilon_p/k = 1500$ K, $\delta_p/\sigma = 0.43$, $V_w/V_p = 5$, $\gamma = 180.88$ mol/m^3). The inset is a zoom view of the phase behavior at high temperatures.

4. Results and discussion

Using the PR-C equation of state, Eq. (1), the equilibrium fluid phase configurations inside different porous media were investigated for two hypothetical systems. System I refers to toluene ($\sigma = 0.57$ nm) adsorption in a homogeneous porous medium characterized by a pore radius of 15 nm, specifying $\varepsilon_p/k = 1500$ K and $\delta_p/\sigma = 0.43$. Another specification is related to the bulk region volume (V_w), i.e., the total volume available to bulk phases, and the confining region volume (V_p), i.e., the total pore volume. The V_w/V_p ratio was set to 5, which is consistent with an adsorption column packed with porous particles [19], assuming that the fluid outside the particles behaves as in a bulk phase.

Figs. 1–3 show the phase configuration of system I as a function of temperature, fixing the global fluid density (γ), i.e., the relation between the total mole number of the fluid and the total volume of the system, in both bulk and confining regions (γ was set to 180.88 mol/m^3). Fig. 1 shows that, at relatively high temperatures, there is only one bulk phase and one adsorbed phase (named as adsorbed phase 1). Decreasing T, adsorption is favored and the density of adsorbed phase 1 increases up to a threshold temperature (around 456 K), below which another adsorbed phase is formed (named as adsorbed phase 2), much denser than the former one. The onset of this dense, liquid-like adsorbed phase

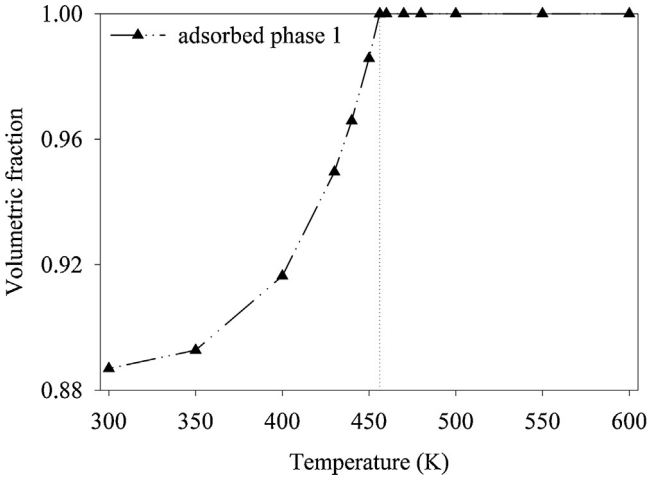

Fig. 2. Occupation of the confining region in system I as a function of temperature ($r_p/\sigma = 26.48$, $\varepsilon_p/k = 1500$ K, $\delta_p/\sigma = 0.43$, $V_w/V_p = 5$, $\gamma = 180.88$ mol/m^3).

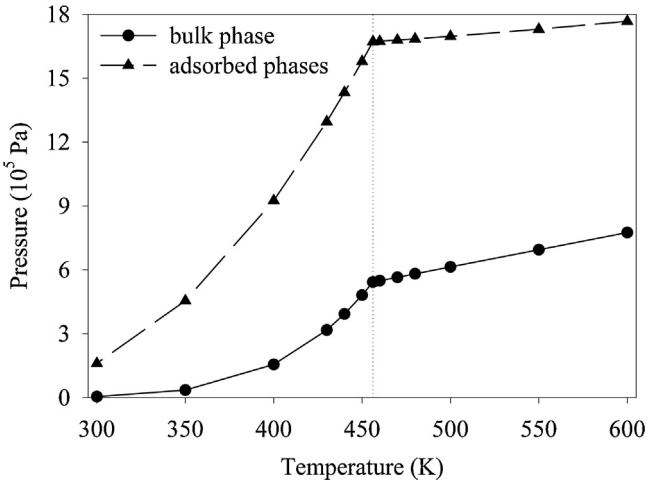

Fig. 3. Pressure in the fluid regions of system I as a function of temperature ($r_p/\sigma = 26.48$, $\varepsilon_p/k = 1500$ K, $\delta_p/\sigma = 0.43$, $V_w/V_p = 5$, $\gamma = 180.88$ mol/m^3).

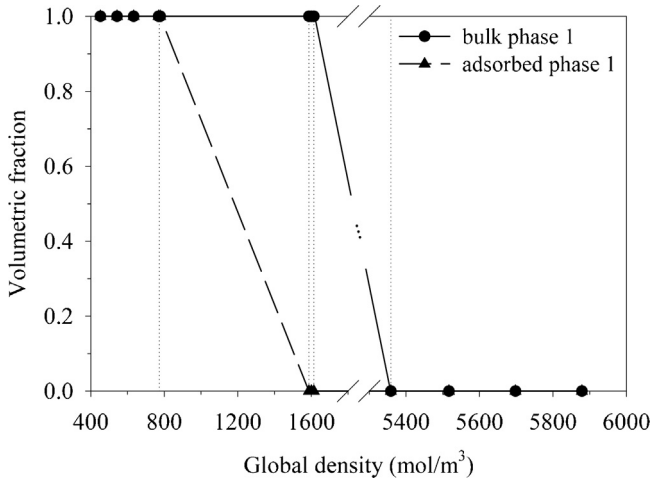

Fig. 5. Occupation of the fluid regions in system I as a function of global fluid density ($r_p/\sigma = 26.48$, $\varepsilon_p/k = 1500$ K, $\delta_p/\sigma = 0.43$, $V_w/V_p = 5$, $T = 550$ K).

at lower temperatures is analogous to the capillary condensation phenomenon in adsorption measurements [1]. From this point on, decreasing T causes reduction in the density of adsorbed phase 1 and increase in the density of adsorbed phase 2, while the first phase is gradually replaced by the second one in the confining region (Fig. 2). Fig. 3 shows the pressures in the bulk and confining regions of system I as function of temperature. As T decreases, pressure is reduced in both regions, as expected, and this effect is more pronounced when adsorbed phase 2 is present, due to its higher density. The pressure is higher in the confining region than in the bulk region, which was also predicted by molecular simulations of argon confined in slit pores [20].

Figs. 4–6 show the effect of the global fluid density on the phase configuration of system I, at the temperature of 550 K. For relatively low densities, there is only one bulk phase and one adsorbed phase, both named as 1 (Fig. 4). Increasing the global density up to a limit (around 773 mol/m^3), density and pressure in both fluid regions increase (Figs. 4 and 6). An additional increase in global density causes the formation of another adsorbed phase (named as 2), which gradually replaces adsorbed phase 1 in the confining region (Fig. 5), leading the system to a new two-phase configuration (in a narrow global density range, around 1600 mol/m^3). Afterwards, the increase in global density causes the gradual replacement of bulk phase 1 by a denser one (named as 2) in the same region. It should

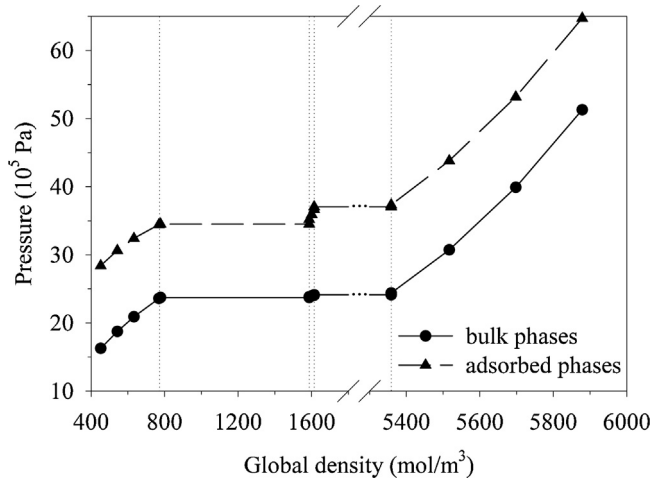

Fig. 6. Pressure in the fluid regions of system I as a function of global fluid density ($r_p/\sigma = 26.48$, $\varepsilon_p/k = 1500$ K, $\delta_p/\sigma = 0.43$, $V_w/V_p = 5$, $T = 550$ K).

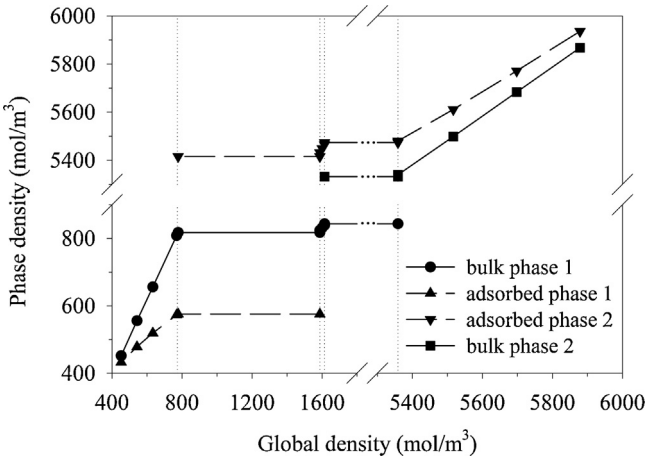

Fig. 4. Density of the fluid phases in system I as a function of global fluid density ($r_p/\sigma = 26.48$, $\varepsilon_p/k = 1500$ K, $\delta_p/\sigma = 0.43$, $V_w/V_p = 5$, $T = 550$ K).

be noted that the density of each phase and the pressure in each fluid region are invariant when there are three phases in the system. This is in agreement with the extended Gibbs phase rule, Eq. (4). For one component distributed in two regions containing three phases, there is only one degree of freedom, which was eliminated with the specification of temperature in Figs. 4–6.

System II refers to the adsorption of an equimolar quaternary mixture (n-butane, n-pentane, n-hexane, and n-heptane) in a structurally heterogeneous porous medium, characterized by two pore radii: 20 nm (with a confining volume $V_{p,1}$) and 15 nm (with a confining volume $V_{p,2}$). The volume relation $V_w/V_{p,1}/V_{p,2} = 11.2/1.8/1.0$ is specified in such a way that the total pore length is the same for both pore sizes. The molecule–wall interaction parameters of each component were specified according to Table 4 (the same values were assigned to both pore sizes, i.e., the porous

Table 4
Molecule–wall interaction parameters of each component in system II.

Component	σ_i (nm)	$\varepsilon_{p,i}/k$ (K)	$\delta_{p,i}/\sigma_i$
n-Butane	0.52	1000	0.5
n-Pentane	0.56	2000	0.5
n-Hexane	0.59	3000	0.5
n-Heptane	0.63	4000	0.5

Table 5
Configuration of fluid phases in system II for a global fluid density of 1012.17 mol/m^3 (values of $\varepsilon_{p,i}$ and $\delta_{p,i}$ shown in Table 4; $V_w/V_{p,1}/V_{p,2} = 11.2/1.8/1.0$, $T = 230$ K).

Pore radius (nm)	Phase	Density (kg/m^3)	Pressure (10^5 Pa)	Volumetric fraction	Mole fractions			
					n-Butane	n-Pentane	n-Hexane	n-Heptane
∞	1 (Bulk gas)	0.1	0.04	1.00	0.855	0.123	0.019	0.003
20	2 (Gas-like)	23.8	15.21	0.69	0.183	0.261	0.281	0.275
20	3 (Liquid-like)	700.3	15.21	0.31	0.258	0.255	0.260	0.227
15	4 (Liquid-like)	700.6	28.50	0.84	0.237	0.235	0.277	0.251
15	5 (Liquid-like)	697.3	28.50	0.16	0.292	0.313	0.068	0.327

Table 6
Configuration of fluid phases in system II for a global fluid density of 1335.06 mol/m^3 (values of $\varepsilon_{p,i}$ and $\delta_{p,i}$ shown in Table 4; $V_w/V_{p,1}/V_{p,2} = 11.2/1.8/1.0$, $T = 230$ K).

Pore radius (nm)	Phase	Density (kg/m^3)	Pressure (10^5 Pa)	Volumetric fraction	Mole fractions			
					n-Butane	n-Pentane	n-Hexane	n-Heptane
∞	1 (Bulk gas)	0.1	0.04	1.00	0.852	0.121	0.025	0.002
20	2 (Gas-like)	23.7	15.22	0.16	0.177	0.256	0.293	0.274
20	3 (Liquid-like)	700.7	15.22	0.84	0.238	0.230	0.316	0.216
15	4 (Gas-like)	32.3	19.68	0.41	0.172	0.256	0.294	0.278
15	5 (Liquid-like)	696.9	19.68	0.59	0.282	0.300	0.082	0.336

medium was considered chemically homogeneous). Other specifications were the temperature (230 K) and the global fluid density (1012.17 or 1335.06 mol/m^3).

Table 5 shows the fluid phase equilibrium condition predicted for system II, setting the global fluid density to 1012.17 mol/m^3. Most of the fluid mass is distributed between the confining regions, resulting in a bulk phase with very low density/pressure, where the components with the highest values of parameter $\varepsilon_{p,i}$ are present in the lowest concentrations, due to their preferential adsorption. The fluid pressure increases as the pore size decreases. Inside the widest pore type, a low density (gas-like) phase and a high density (liquid-like) phase are predicted to occur. Inside the narrowest pore type, the existence of two high density phases with different compositions is predicted. Three of the adsorbed phases have compositions close to the global composition; however, the concentration of n-hexane in phase 5 is substantially smaller. Moreover, in the widest pore type, the gas-like phase is poorer in the lightest fluid component (n-butane) and richer in the other components than the liquid-like phase. This unusual phase behavior is possible because of the confinement effects, which give rise to different levels of entropic and energetic contributions. The fluid molecules are close to random distribution in the liquid-like phase because of its high density, but the low density, gas-like phase allows for a preferential occupation of the pore wall vicinity by the heaviest components, to which much higher energies of molecule–wall interaction were assigned.

Fig. 7 illustrates how the adsorbed phases of system II occupy the confining regions, for the global fluid density of 1012.17 mol/m^3. In Fig. 7, it is considered that the pores are vertically oriented. Despite the fact that the influence of the gravity field was not considered in the calculations explicitly, its expected effect is that phases with the lowest mass densities are located above those with the highest densities. There is a vertical region of the porous medium in which a gas-like phase and a liquid-like phase are present, similarly to a GOC transition region in an oil reservoir [3]. This suggests how transition regions in porous media can be represented with the kind of model of this work, which explicitly considers the main effects of confinement.

Table 6 shows the fluid phase equilibrium condition predicted for system II and Fig. 8 shows the adsorbed phases configuration in this system, setting the global fluid density to 1335.06 mol/m^3. Comparing with Table 5 and Fig. 7, the increase in global density resulted in the substitution of one liquid-like phase in the narrowest pore type by a gas-like phase (the remaining liquid-like phase in this pore type retained the peculiar composition of phase 5 in Table 5). This unexpected behavior is associated to a partial

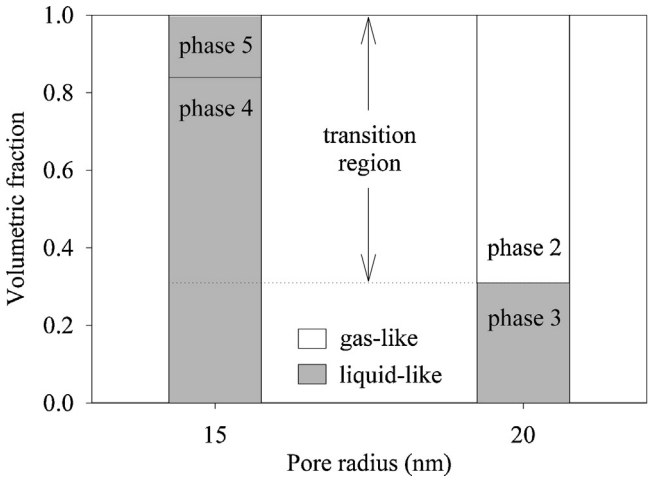

Fig. 7. Configuration of adsorbed phases in system II for a global fluid density of 1012.17 mol/m^3 (values of $\varepsilon_{p,i}$ and $\delta_{p,i}$ shown in Table 4, $V_w/V_{p,1}/V_{p,2} = 11.2/1.8/1.0$, $T = 230$ K). The transition region is the vertical section of the porous medium where phases with different densities coexist.

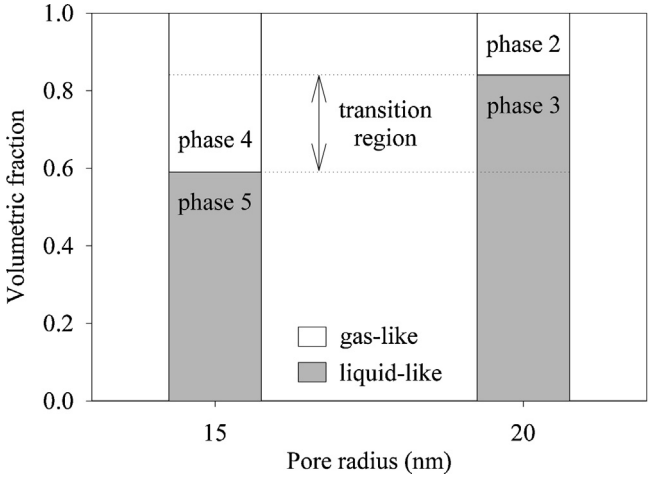

Fig. 8. Configuration of adsorbed phases in system II for a global fluid density of 1335.06 mol/m^3 (values of $\varepsilon_{p,i}$ and $\delta_{p,i}$ shown in Table 4, $V_w/V_{p,1}/V_{p,2} = 11.2/1.8/1.0$, $T = 230$ K). The transition region is the vertical section of the porous medium where phases with different densities coexist.

condensation of the gas-like phase in the widest pore type (phase 2). As a consequence, the transition region has shrunk with the increase in global density. Other complex behaviors can derive from confinement effects and would be easily handled with the multiphase equilibrium algorithm used in this work.

5. Conclusions

Commonly used cubic equations of state were extended to the modeling of fluids confined in porous media. The extended models are applicable to both confined and bulk phases, providing a consistent description of adsorption systems, including those in which the adsorbents have either size or chemical heterogeneity. A model based on the Peng–Robinson equation of state was used in a conventional multiphase equilibrium calculation algorithm to establish the fluid phase equilibrium condition inside different porous media, a matter of difficult experimental investigation. For a heterogeneous porous medium characterized by two pore sizes, the existence of a transition region was predicted, in which two phases with very different densities were present at the same vertical level, trapped in different pores, similarly to what is believed to occur in natural oil reservoirs. Although the case studies presented in this work address simple fluid compositions and pore distributions, our approach allows for dealing with more complex systems with a reasonable rise in computational cost, similar to that of increasing the number of phases in flash calculations performed with conventional equations of state.

List of symbols

a	conventional energy parameter of the equations of state
a_p	confinement-modified energy parameter of the equations of state
b	conventional volume parameter of the equations of state
b_p	confinement-modified volume parameter of the equations of state
c, d	constants
E_{conf}	configurational energy
F	Helmholtz energy
F_p	fraction of the confined molecules subject to the pore wall attractive field
F_{pa}	value of F_p for random distribution of the molecules inside the pore
f_{PR}, f_S	functions of temperature
k	Boltzmann constant
n	number of moles
N	number of molecules
N_{av}	Avogadro number
N_c	coordination number
NC	number of components
NF	number of fluid phases
NL	number of degrees of freedom
NR	number of regions available to the fluid
P	pressure
q	internal partition function of one molecule
Q	canonical partition function
R	ideal gas constant
r_p	pore radius
T	absolute temperature
v	molar volume
V	total volume
V_f	free volume
V_p	confining region volume
V_w	bulk region volume
x	mole fraction

Greek letters

α_{PR}	function of temperature and acentric factor for the Peng–Robinson equation of state
α_S	function of temperature and acentric factor for the Soave equation of state
γ	global fluid density
Δ	Kronecker delta function
δ_p	square well width of the molecule–wall interaction potential
ε	square well depth of the molecule–molecule interaction potential
ε_p	square well depth of the molecule–wall interaction potential
η	distribution factor
θ	geometric term in the expression of F_p
λ	de Broglie wavelength
μ	chemical potential
ρ	molecular fluid density
ρ_{max}	confinement-modified molecular packing density
σ	molecular diameter
φ	volumetric fraction
ψ	confinement-modified attractive part of the equations of state

Superscript

b	bulk property

Subscripts

g, s	regions available to the fluid
h, t	fluid phases
i, j	components

Acknowledgements

The authors acknowledge the financial support of CNPq/Brazil during the early stages of this research. From January 2013, work on this publication was made possible by a NPRP award (NPRP 5-344-2-129) from the Qatar National Research Fund (a member of The Qatar Foundation). The statements made herein are solely the responsibility of the authors.

References

[1] L.D. Gelb, K.E. Gubbins, R. Radhakrishnan, M. Sliwinska-Bartkowiak, Rep. Prog. Phys. 62 (1999) 1573–1659.
[2] J.K. Singh, S.K. Kwak, J. Chem. Phys. 126 (2007) 024702-1–024702-8.
[3] R.J. Wheaton, SPE Reservoir Eng. 6 (1991) 239–244.
[4] D. Frenkel, B. Smit, Understanding Molecular Simulation, second ed., Academic Press, New York, 2002.
[5] H.C. Van Ness, Ind. Eng. Chem. Fundam. 8 (1969) 464–473.
[6] M. Schoen, D.J. Diestler, J. Chem. Phys. 109 (1998) 5596–5606.
[7] G.J. Zarragoicoechea, V.A. Kuz, Phys. Rev. E 65 (2002) 021110-1–021110-4.
[8] H. Kim, W.A. Goddard III, K.H. Han, C. Kim, E.K. Lee, P. Talkner, P. Hänggi, J. Chem. Phys. 134 (2011) 114502-1–114502-11.
[9] E. Fathi, I.Y. Akkutlu, Transp. Porous Med. 80 (2009) 281–304.
[10] L. Travalloni, M. Castier, F.W. Tavares, S.I. Sandler, Chem. Eng. Sci. 65 (2010) 3088–3099.
[11] L. Travalloni, M. Castier, F.W. Tavares, S.I. Sandler, J. Supercrit. Fluids 55 (2010) 455–461.
[12] V. De Grandis, P. Gallo, M. Rovere, J. Mol. Liq. 134 (2007) 90–93.
[13] S.I. Sandler, Chem. Eng. Education Winter (1990) 12–19.
[14] S.I. Sandler, Chem. Eng. Education Spring (1990) 80–87.
[15] G.E. Mueller, Powder Technol. 159 (2005) 105–110.
[16] V.F. Cabral, M. Castier, F.W. Tavares, Chem. Eng. Sci. 60 (2005) 1773–1782.
[17] W. Murray, Numerical Methods for Unconstrained Optimization, first ed., Academic Press, New York, 1972.
[18] M.L. Michelsen, Fluid Phase Equilib. 9 (1982) 1–19.
[19] T.L.P. Dantas, F.M.T. Luna, I.J. Silva Jr., A.E.B. Torres, D.C.S. Azevedo, A.E. Rodrigues, R.F.P.M. Moreira, Chem. Eng. J. 172 (2011) 698–704.
[20] Y. Long, J.C. Palmer, B. Coasne, M. Śliwinska-Bartkowiak, K.E. Gubbins, Phys. Chem. Chem. Phys. 13 (2011) 17163–17170.